JOURNAL DE PHYSIQUE IV
Colloque C8, supplément au Journal de Physique I, Volume 3, décembre 1993

Resolution effects and analysis of small-angle neutron scattering data

J.S. PEDERSEN

Department of Solid State Physics, Risø National Laboratory, 4000 Roskilde, Denmark

A discussion of the instrumental smearing effects for small-angle neutron scattering (SANS) data sets is given. It is shown that these effects can be described by a resolution function, which describes the distribution of scattering vectors probed for the nominal values of the scattering vector. The resolution function is independent of the scattering cross section of the sample and can be calculated once and for all for any instrumental setting. For scattering from isotropic system the resolution function allows the smeared intensity to be calculated by computing only one numerical integral. It is discussed how the resolution function can be calculated analytically, determined by Monte Carlo simulations, and measured. It is demonstrated that for typical SANS setups, the resolution function can be described by a Gaussian function to a good approximation. The incorporation of the function in computer programs for least-squares fits of known cross sections and for indirect Fourier transformations is discussed. Finally, some examples are given which demonstrate the application.

1 Introduction

Most small-angle neutron scattering (SANS) setups are composed of the following components: A mechanical velocity selector, two collimating pinholes, and a two-dimensional position sensitive detector. Modern instruments are often very flexible and allow variation of the neutron wavelength, the collimation, and the sample-detector distance. This makes it possible to cover a broad range of scattering vectors (2–3 orders of magnitude) by measuring with several different instrumental settings.

Most experimental small-angle neutron scattering data sets are significantly influenced by instrumental resolution effects. This is particularly clear when the scattering curve is measured for different instrumental settings with overlapping ranges of scattering vectors [1-5]. If the smearing effects are not included in the data analysis it will inevitably lead to systematic errors in the results and the derived parameters [6]. Therefore the general recommendation must naturally be to include the instrumental smearing effects in the data analysis, but for the analysis of overlapping ranges of scattering vectors it is absolutely indispensable.

For scattering from isotropic systems, where the scattering intensity can be described as a function of only the modulus q of the scattering vector $\mathbf{q}$, the smearing effects can be incorporated in the data analysis by the traditional smearing integrals (see *e.g.* [3,7,8]) using the slit length, slit width, and wavelength distribution (weighting) functions. This requires the calculation of three numerical integrals which makes the calculations quite time consuming, for example when performing least-squares fits of simple analytical expressions to the data [9]. For small-angle neutron scattering

setups it is more convenient to express the smearing in terms of a resolution function $R(\langle q\rangle, q)$ [10], which describes the distribution of scattering vectors q that contribute to the scattering for the nominal scattering vector $\langle q\rangle$. With this, the measured intensity $I(\langle q\rangle)$ is related to the cross section $d\sigma(q)/d\Omega$ by the integral:

$$I(\langle q\rangle) = \int R(\langle q\rangle, q)\frac{d\sigma(q)}{d\Omega}\, dq. \tag{1}$$

The resolution function $R(\langle q\rangle, q)$ contains contributions from the finite collimation, the spatial resolution of the detector, and the wavelength distribution. For data deduced from a two-dimensional spectrum recorded with a position sensitive detector by azimuthal averaging, there is an additional contribution from the finite size of the bins on the q scale, when grouping the pixels of the detector.

In the following section it will be shown that the contributions to the resolution function can be described with Gaussian functions to a very good approximation. This will be demonstrated by both Monte Carlo simulations and by direct measurements. It will also be shown that the methods for calculating the width of the resolution function [10] give results which agree well with the width determined by the measurements and the simulations. It will also be discussed how the resolution function is incorporated in the data analysis programs. Finally, some examples of analysis of experimental data, in which the resolution function is used, will be given.

First it will be assumed that the contributions to the resolution function are strictly Gaussian, so that the combined resolution function can be calculated analytically [10]. In reality the scattering geometry is three-dimensional and therefore the resolution function describes the distribution of scattering vectors in three dimensions. However, the application of this resolution function is only necessary when analyzing data from systems with Bragg-like reflections. This resolution function has recently been calculated [11] and it is presently being applied for analyzing data from FeGe and MnSi. In the present paper three-dimensionally well-ordered systems will not be considered and therefore the direction perpendicular to the Ewalds sphere can be neglected. The two-dimensional resolution function, which will be considered, is the projection of the three-dimensional one on the Ewalds sphere.

Using a coordinate system with the two axis, respectively, parallel and perpendicular to nominal scattering vector, one has for small scattering angles $\langle \mathbf{q}\rangle = (2\langle k\rangle\langle\theta\rangle, 0)$. The nominal values are indicated as $\langle\cdot\rangle$. The parameter k is the wave vector and θ is the scattering angle. The resolution function describes the distribution of scattering vectors around $\langle \mathbf{q}\rangle$. A general scattering vector is $\mathbf{q} = (q_1, q_2) = (2k\theta, 2k\delta)$, where δ is the scattering angle in the direction perpendicular to $\langle \mathbf{q}\rangle$. The vector $\mathbf{q}$ can be expanded to first order around $\langle \mathbf{q}\rangle$ in the wave vector k and the two angle parameters $\Delta\theta = \theta - \langle\theta\rangle$ and δ, which describe, respectively, the deviation in scattering angle parallel and perpendicular to $\langle \mathbf{q}\rangle$:

$$\Delta\mathbf{q} = \mathbf{q} - \langle \mathbf{q}\rangle = \begin{pmatrix} 2\langle\theta\rangle\,\Delta k + 2\langle k\rangle\Delta\theta \\ 0 + 2\langle k\rangle\delta \end{pmatrix} = \begin{pmatrix} \langle q\rangle\,\Delta k/\langle k\rangle + 2\langle k\rangle\Delta\theta \\ 2\langle k\rangle\delta \end{pmatrix}. \tag{2}$$

The distribution of $\Delta k/\langle k\rangle$ is provided by the mechanical velocity selector and the distributions of $\Delta\theta$ and δ are given by the collimation and the spatial resolution of the detector. The distributions of $\Delta k/\langle k\rangle$ and $\Delta\theta$ are to a good approximation independent and therefore the distribution of Δq_1 is the convolution of the distribution of $\langle q\rangle\,\Delta k/\langle k\rangle$ and of $2\langle k\rangle\,\Delta\theta$ [12]. For Gaussians the resulting function is Gaussian with the width squared equal to the sum of the width squared of the two contributions:

$$\sigma_1(\langle q\rangle)^2 = \langle q\rangle^2\,\sigma(\Delta k/\langle k\rangle)^2 + 4\langle k\rangle^2\,\sigma(\Delta\theta)^2. \tag{3}$$

In this equation the widths have been expressed as the variances (σ) of the distributions. One has $\sigma = W/2\sqrt{2\ln 2}$, where W is the full-width-half-maximum (FWHM) value. Note that the first

term increases with $\langle q \rangle$ whereas the second term is constant. In the direction perpendicular to $\langle q \rangle$ one has only the constant term:

$$\sigma_2(q) = 2\langle k \rangle \delta. \tag{4}$$

The resulting Gaussian resolution function is:

$$R(\langle \mathbf{q} \rangle, \mathbf{q}) = \frac{1}{2\pi\sigma_1\,\sigma_2} \exp[-\frac{1}{2}(\frac{(q_1 - \langle q \rangle)^2}{\sigma_1^2} + \frac{q_2^2}{\sigma_2^2})]. \tag{5}$$

For isotropic data, which are azimuthally averaged, the appropriate resolution function can be obtained from eq. (5) by azimuthal integration. The result is [10] (setting $q = q_1$):

$$R(\langle q \rangle, q) = \frac{q}{\sigma_1^2} \exp[-\frac{1}{2}\frac{(q^2 + \langle q \rangle^2)}{\sigma_1^2}]\, I_0(q\,\langle q \rangle/\sigma_1), \tag{6}$$

where I_0 is the modified Bessel function of first kind and zeroth order. This is the resolution function entering eq. (1).

2 Determination of the resolution function

In this section methods for determining the two contributions to the resolution function from, respectively, the spread in wave vector and from the spread in scattering angle, are described. The two distributions will be considered separately and the combined effect will be taken as given by eq. (3). In the following it is shown that the distributions can be determined by calculations, simulations, and direct measurements. Note that at $\langle q \rangle = 0$ the contribution from the wave vector to the resolution function vanishes (3). Therefore the spread in scattering angles can be determined as the profile of the direct beam on the detector.

2.1 Calculations

The distribution of wave vectors are given by the dimensions and rotation speed of the mechanical velocity selector. The neutrons have to have a velocity which matches velocity defined by the turn of the helical slots of the velocity selector. However, the finite width of the slots leads ideally to a triangular distribution of velocities (and of wave vectors). The wave vector $\langle k \rangle$ is given by:

$$\langle k \rangle = 2\pi\, m\omega R/(h\alpha), \tag{7}$$

where m is the neutron mass, ω the angular velocity of the rotor, R the distance from the center of the rotor to the beam, and α the inclination angle of the slots relative to the beam direction. The parameter h is Planck's constant. The spread is given by:

$$\Delta k/\langle k \rangle = \alpha\, S\, d/(S^2\alpha^2 - d^2), \tag{8}$$

where d is the width of the slots and S is the length of the selector.

As already mentioned the contribution from the spread in the scattering angle is given by the profile of the direct beam on the detector. It can be calculated as done in reference [10]. The profile is given by the contribution from the finite collimation convoluted with the spatial resolution of the detector. The width squared is obtained by adding the square of the widths. It is straight forward to derive the expression for the width from the expressions in reference [10].

2.2 Monte Carlo simulations

The Monte Carlo method is a very useful tool that allows to simulate ideal "experiments" or "measurements", for which the conditions are precisely known. It is in principle straight forward to perform the simulations, but in order to have a reasonably fast algorithm care has to be taken that as many events as possible are accepted.

The wave vector distribution on the sample position depends to some degree on the collimation, and to include this effect, the collimation has to be incorporated in the simulation. In order to have many accepted events the simulations have to be done "backwards". First the direction of the neutron is chosen by picking out randomly a position on both of the two apertures. For circular apertures with radius r this is done by having one uniformly distributed parameter between $-r$ and $+r$ for each of the two coordinates x and y. Only the events with $r^2 \geq x^2 + y^2$ are accepted. Next the exit position of the neutron with respect to the slots of the mechanical velocity selector is chosen. The wave vector of the neutron is chosen in the appropriate range from a distribution that represents the spectrum of the reactor or the cold source. It can now be calculated if the neutron, with the given rotation speed of the selector, was within the same slot at the entrance of the selector. If this is the case the event is accepted. The procedure is repeated and the events are accumulated in a histogram memory.

The profile of the beam on the detector can be determined in a similar way. The positions on the two apertures are chosen randomly and the position on the detector of the neutron is calculated. A random component corresponding to the detector resolution is added in both the x and y direction. The detector resolution has typically a Gaussian distribution and the random components are chosen with this distribution. The events are accumulated in a histogram memory for which the bin size is identical to the pixel size of the detector. Note that the direct beam profile does not depend on the value of the wave vector.

2.3 Measurements

The wavelength or wave vector distribution can be measured by a time-of-flight technique. A chopper has to be placed at the entrance to the instrument, so that one gets a flight path as long as possible in order to have good resolution. For the same reason the pulse duration has to be as short as possible. The time of the arrival of the neutrons to the detector is recorded and stored in a histogram memory. The time is converted to wave vector using the known distance from the chopper to the detector.

Alternatively the wave vector distribution can be measured by placing a diffractometer with a crystal and a detector arm after the sample aperture. The distribution is obtained by doing a conventional $\theta - 2\theta$ scan and by applying Bragg's law: $k = \sin\theta/(2\tau)$, where τ is the reciprocal lattice vector of the crystal.

The direct beam profile can simply be measured by the detector after removing the beamstop. In order to avoid saturating and destroying the detector the beam has to be attenuated. The usual attenuator is a cadmium plate with uniformly distributed small holes.

2.4 Examples

In this section some examples of applications of the methods, described in the previous sections, are given. The measured wave vector distribution of the small-angle neutron scattering instrument at Risø National Laboratory [13] is shown in Fig. 1. It has been measured by a diffractometer at the sample position. The curve in the figure is a Gaussian with the FWHM value $\Delta k/\langle k \rangle = 0.18$. The Gaussian gives a reasonable approximation to the measured distribution with small deviations in the tails.

Figure 2 shows the radial intensity distribution of the direct beam of the Risø instrument. The instrument has circular apertures. For the measurements the radius of the source and sample apertures were, respectively, $r_1 = 0.8$ cm and $r_2 = 0.4$ cm. The distance between the two pinholes was $L = 300$ cm and the sample-detector distance was $l = 300$ cm. The detector resolution was 0.8

cm and the size of the pixels is 0.5 × 0.5 cm^2. The curve is from a fit of a Gaussian. The resulting FWHM value is 1.62 cm. The agreement with the measured points is very good. The width calculated analytically as described in section 2.1 gives 1.53 cm, which is in reasonable agreement with the value for the experimental profile.

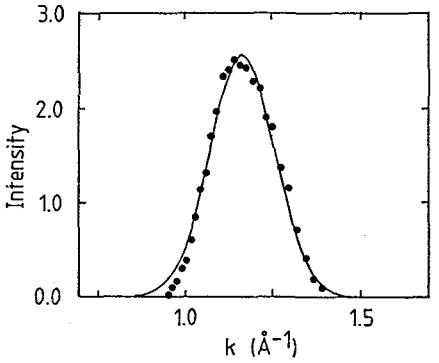

Fig. 1: The measured wave vector distribution of the mechanical velocity selector at the Risø small-angle scattering instrument. The full curve is a Gaussian with the FWHM value $\Delta k/\langle k\rangle = 0.18$.

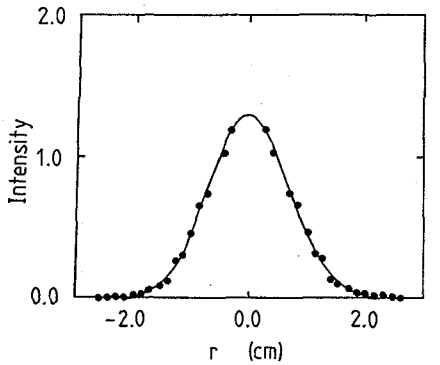

Fig. 2: The radial intensity distribution of the direct beam profile for the Risø instrument. The parameters for the setup are given in the text. The curve is from a fit of a Gaussian.

Figure 3 shows the radial intensity distribution of the direct beam profile from a Monte Carlo simulation. The parameters for the setup are identical to those for the experimental profile shown in Fig. 2. The curve is from a fit of a Gaussian, which agrees very well with the simulation. The width is 1.65, which is nearly identical to the experimental value.

From the examples given in the present section it can be concluded that Gaussian functions describe well both the wave vector distribution and the direct beam profile. Therefore the combination of the two effects to the resolution function can be done as described in the introduction. The squared width of the resolution function is given by eq. (3).

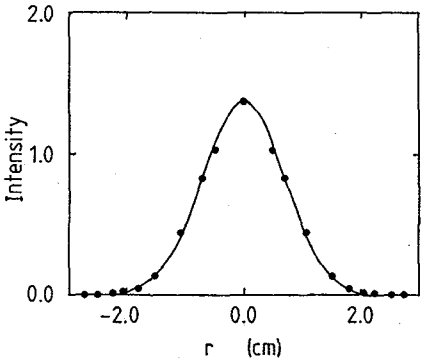

Fig. 3: The radial intensity distribution of the direct beam profile from a Monte Carlo simulation. The parameters for the setup are given in the text and they are identical to those for the experimental profile shown in Fig. 2. The curve is from a fit of a Gaussian.

3 Implementation

When the smearing with the resolution function is implemented in a computer program for data analysis a numerical integral representing eq. (1) has to be calculated for each value of the nominal scattering vector $\langle q\rangle_i$:

$$I(\langle q\rangle_i) = \sum_{j=1}^{N} R(\langle q\rangle_i, q_j)\frac{d\sigma}{d\Omega}(q_j)\,\Delta q, \tag{9}$$

where q_j are equidistant values in the interval $[\langle q\rangle_i - 3\sigma_i; \langle q\rangle_i + 3\sigma_i]$, and $\sigma_i = \sigma_1(\langle q\rangle_i)$ (eq. 3). N is the number of points in the integral, and $\Delta q = q_j - q_{j-1}$. Typically one needs $N = 10 - 20$ in order to have a sufficient accuracy of the convolution. This means that the cross section has to be calculated for N times as many scattering vectors as one has in the measured data. For

performing least-squares fits [10] or indirect Fourier transformations (IFT) [6,14] one can save a lot of computing time by calculating the resolution functions before starting the fits. The resolution function and the q values can be saved in matrices ($R_{i,j}$ and $q_{i,j}$) and used for all the calculations during the least-squares fitting or for smearing all the basis functions in the IFT.

For least-squares fits of involved cross sections with many parameters it is the calculation of the cross section which takes the major part of the time. In most situations the range of the resolution function (usually taken as 6 σ_i) is much larger than the separation between the experimental points. When using eq. (9) for calculating the convolution one calculates the cross section in nearly the same range for neighboring values of $\langle q \rangle$. This means that the cross section is calculated for more q values than necessary. In this situation it is advantageous to use a master curve for the cross section. It should be calculated in the range from $\langle q \rangle_1 - 3\sigma_1$ to $\langle q \rangle_M - 3\sigma_M$, where $\langle q \rangle_1$ and $\langle q \rangle_M$ are, respectively, the smallest and the largest value of $\langle q \rangle$. The master curve should be generated before calculating the smearing integrals (9). In the least-squares routine this is easily done by making a subroutine call before each calculation of chi-squared. The values of the cross section, which are required for evaluating (9), can be determined by linear interpolation.

Alternatively one can compute the resolution function for the q values which are used for calculating the master curve [15]. Then one has to keep track of the indices of the points in the master curve which enter the smearing integrals. This is easily done by storing for each $\langle q \rangle_j$ value the index of the first and last point in the master curve. This method has been used for analysis of specular neutron reflectivity data [15].

4 Applications: data analysis

In this section some examples of the application of the Gaussian resolution function will be given. Addition examples can be found in the references [1,2,4-6,10].

4.1 Porod scattering

Copper crystals fatigued at high temperatures develop large cavities at the grain boundaries. For sufficiently large cavities only the Porod region with a q^{-4} scattering is observed in a SANS experiment. An example of this is shown in Fig. 4, where a plot of Iq^4 versus q is displayed [16]. Significant deviations from the ideal behavior (the dotted curve) are observed in particular at low q values. This is due to the increasing importance of the instrumental smearing at low q for the concave, diverging scattering curve. The full curve in the figure is the cross section smeared by instrumental resolution.

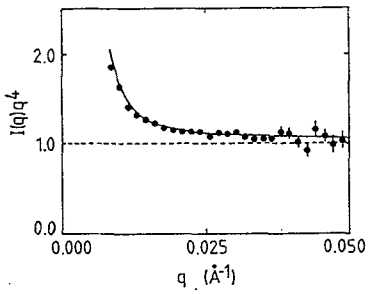

Fig. 4: A Porod plot of the scattering for fatigued copper [16]. The dotted curve is the ideal q^{-4} scattering and the full curve is the intensity smeared by instrumental resolution.

It is clear from the plot that the data can not be fitted properly with a q^{-4} cross section without including the smearing effects. The resolution effects become particular obvious when more than one instrumental setting is used for recording the intensity curve. In this case the Porod plot shows the characteristic upturn at the low-q part of each setting. This has been observed for a granular PVC powders [17].

4.2 The coblock polymer P85 in aqueous solution

The polymer P85 is a triblock polymer of poly(ethylene oxide)-poly(propylene oxide)-poly(ethylene oxide) with the composition $PEO_{25}PPO_{40}PEO_{25}$. At high temperatures (> 5–40°C) the PPO becomes hydrophobic and micelle formation sets in [4]. The phase diagram of the system as a function of polymer concentration and temperature has been studied by the SANS technique [4].

In the present context some of the analysis in the temperature region with spherical micelles is described.

Figure 5 shows the SANS spectrum of 4 wt % P85 dissolved in D_2O at 26°C obtained using three instrumental settings. The data have been analyzed by an indirect Fourier transformation [14] and the resulting distance distribution function $p(r)$ is also shown in the figure. It is quite similar to $p(r)$ for a system of spheres with finite volume fraction and with hard-sphere interactions [7].

The full curves in Fig. 5 (a) are the fits smeared by instrumental resolution. The broken curve is the non-smeared cross section. Some resolution effects can be observed in the overlap regions and when omitting the resolution function the quality of the fits becomes much worse. The $p(r)$ function suggests that the data can be fitted by a hard-sphere model [4]. Some examples from fitting such a model to the data are shown in Fig. 6 for different polymer concentrations and temperatures. The hard-sphere volume fraction for the examples (a, b, c) are, respectively, 0.13, 0.30, and 0.40. For increasing volume fractions the correlation peak becomes more pronounced and sharper. In the figure one clearly sees the increasing effect of the instrumental resolution as the peak sharpens.

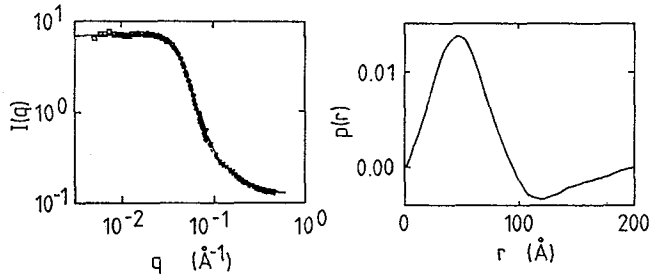

Fig. 5: (a) SANS spectrum [4] of 4 wt % P85 dissolved in D_2O at 26°C obtained using three instrumental settings. (b) The corresponding distance distribution function obtained by IFT.

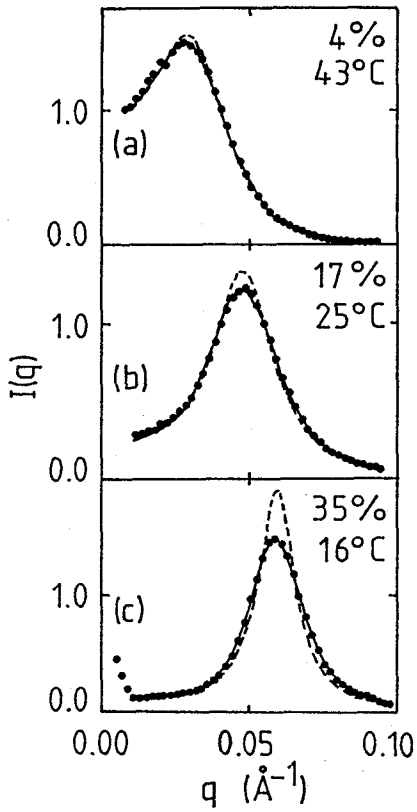

Fig. 6: SANS spectra [4] for 4 (a), 17 (b), and 35 (c) wt. % P85 at respectively 43, 25, and 16°C. The full curves are from fits of a hard-sphere model smeared by instrumental resolution. The broken curves are the ideal model intensities.

4.3 Aggregates of alfalfa mosaic virus coat proteins

The last examples concerns a re-analysis of SANS data from RNA-free aggregates of coat proteins from alfalfa mosaic virus (AMV) recorded by Cusack et al. [18]. In the original publication the authors could not find a model, which gave a satisfactory fit to the data. In the following a model is derived, which turns out to agree very well with the results from x-ray crystallography [19].

The data, shown in Fig. 7, display pronounced oscillations, indicating that the structure is nearly spherical symmetric. The curves in the figure are from an IFT [4]. The oscillations are, as expected, more pronounced in the desmeared (broken) curve. The insert shows the $p(r)$ function. The shape is close to that of a thin spherical shell [4], but with some oscillations, which originate from the internal structure of the shell due to the proteins.

The mass of the aggregate corresponds to 60 proteins in each (T = 1) [18], which gives three proteins on each of the triangles of the icosahedron (see insert in Fig. 8). The results from a fit using such a model, in which the proteins are described as solid spheres, are shown in Fig. 8. In the insert is also shown the resulting position of the proteins. The spheres are from the fit to the SANS

data and the broken curves indicate the proteins as determined by x-ray crystallography. The results from the analysis of the SANS data are in excellent agreement with the x-ray diffraction results.

This completes the examples of applications of the resolution function in the analysis of SANS data. They demonstrate the great usefulness of the concept.

Acknowledgments: I thank D.I. Svergun, A.N. Falcão, K. Mortensen, S. Hansen, and J.G Barker for fruitful discussions, and D.I. Svergun and A.N. Falcão for their comments on the manuscript.

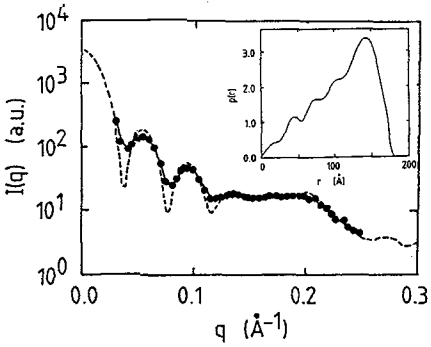

Fig. 7: SANS data [18] from the aggregates of AMV coat proteins. The broken curve is the desmeared curve from an IFT. The full curve is the intensity smeared by instrumental resolution. The insert shows the $p(r)$ function determined by IFT.

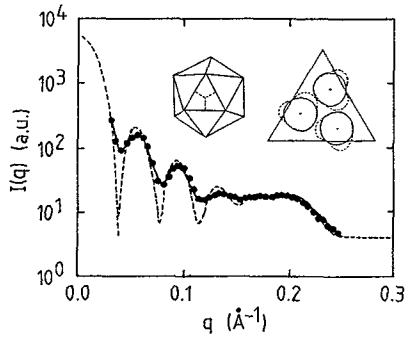

Fig. 8: SANS data [18] from the aggregates of AMV coat proteins. The curves are from the fit of an icosahedral (T=1) model. The inserts show the icosahedron and the position of the proteins on the triangles of the icosahedron.

References

[1] BAUER R., BEHAN M., HANSEN S., JONES G., MORTENSEN K., SÆRMARK T., ØGENDAL L., *J. Appl. Cryst.* **24** (1991) 815.

[2] BAUER R., BEHAN M., CLARKE D., HANSEN S., JONES G., MORTENSEN K., PEDERSEN J. SKOV, *Eur. Biophys. J.* **21** (1992) 129.

[3] SVERGUN D.I., *J. Appl. Cryst.* **24** (1991) 485.

[4] MORTENSEN K., PEDERSEN J. SKOV, *Macromolecules* **26** (1993) 805.

[5] PEDERSEN J. SKOV, *Eur. Biophys. J.* (1993) *In the press.*

[6] HANSEN S., PEDERSEN J. SKOV, *J. Appl. Cryst.* **24** (1991) 541.

[7] GLATTER O., in *Small angle x-ray scattering*, edited by O. Glatter and O. Kratky (1982) (Academic Press).

[8] FEIGIN L.A., SVERGUN D.I., *Structure analysis by small-angle X-ray and neutron scattering* (1987) (Plenum Press).

[9] SJÖBERG B., *J. Appl. Cryst.* **11** (1978) 73.

[10] PEDERSEN J. SKOV, POSSELT D., MORTENSEN K., *J. Appl. Cryst.* **23** (1990) 321.

[11] HARRIS P., PEDERSEN J. SKOV, *to be published* (1993).

[12] HAUGEN E.B., *Probabilistic Approaches to Design* (1968) (Wiley) pp. 84-85.

[13] LEBECH B., *Neutron News* **2** (1990) 7.

[14] GLATTER O., *J. Appl. Cryst.* **10** (1977) 415.

[15] PEDERSEN, J. SKOV, HAMLEY, I.W., *to be published* (1993).

[16] BARKER J.G., WEERTMAN J.R., PEDERSEN, J. SKOV, *to be published* (1993).

[17] SCHERRENBERG R., REYNAERS H.R., VLAK W.A.H.M., MORTENSEN K., PEDERSEN, J. SKOV, *unpublished* (1992).

[18] CUSACK S., MILLLER A., KRIJGSMAN P.C.J., MELLEMA J.E., *J. Mol. Biol.* **145** (1981) 525.

[19] FUKUYAMA K., ABDEL-MEGUID S.D., JOHNSON J.E., ROSSMANN M.G., *J. Mol. Biol.* **167** (1983) 873.